C. Brossard, J.-C. Monnier,
P. Barricau, F.-X. Vandernoot,
Y. Le Sant, F. Champagnat,
G. Le Besnerais
(Onera)

E-mail: Christophe.Brossard@onera.fr

Principles and Applications of Particle Image Velocimetry

In this paper, the principles of two-component Particle Image Velocimetry (PIV) and stereoscopic PIV are first recalled. Recent improvements in the camera calibration procedure for stereoscopic PIV are highlighted. The advantages of the PIV technique are illustrated through different studies performed in Onera laboratories for non-reacting or reacting flows, and various issues raised by the nature of fluid, flow dynamics, spatial and temporal resolutions, as well as data utilization, are examined. Finally, recent advances in the technique, time-resolved PIV and tomographic PIV, as well as potential gains from novel processing and post-processing algorithms, are presented.

Introduction

Particle Image Velocimetry appeared 25 years ago and since then has become an essential measurement technique in fluid mechanics laboratories in both research institutes and industry. Papers related to PIV have represented approximately half of the total papers presented in the Lisbon International Symposia on Applications of Laser Techniques to Fluid Mechanics held since 2000 [1]. This success, boosted by the progress in laser technologies as well as electronic image recording, can be explained by the large quantity of information that can be recorded instantaneously and simultaneously, for a reasonable implementation effort, compared to other measurement techniques. It is also related to the development of several commercial systems that have made the technique easily available worldwide, for a very large variety of applications, ranging from microfluidic scales ($\sim$ a few hundred microns) to large fields ($\sim$ 1 m) in wind tunnels. This spectacular development has been largely supported through collaborative networks such as EUROPIV or PIV Challenge ([2-5]), set up to foster international cooperation and organize worldwide comparison of algorithm performances.

The purpose of this paper is not to provide a detailed course on PIV. We recommend that readers with that aim in mind consult the reference books in the field [6] or follow one of the high quality courses fully or partly dedicated to PIV, such as the ones proposed by the DLR (Deutsches Zentrum für Luft- und Raumfahrt, [7]), VKI (Von Karman Institute, [8]) or AFVL (Association Francophone de Vélocimétrie Laser, [9]). Rather, after a brief reminder of the principles of the technique, its high potential will be illustrated using some selected studies performed at Onera. We will then present the most significant directions of progress that this continuously evolving technique has followed recently.

Fundamentals of PIV

Principles of two-component PIV (2C-PIV)

Based upon the definition of velocity, i.e. the first derivative of position with respect to time, the technique consists in measuring the displacement of fluid (Δx) over a given time interval (Δt). The position of the fluid is imaged through the light scattered by liquid or solid particles illuminated by a laser light sheet. In most applications, such particles are not naturally present in the flow which, therefore, has to be seeded with tracer particles, assumed to be sufficiently small and light to move with local flow velocity. Figure 1 shows a typical standard two-component PIV (2C-PIV) setup. A plane within the flow is illuminated twice by means of two superimposed laser light sheets. The light scattered by the particles is recorded on two separate frames on a special cross-correlation CCD camera sensor. For evaluation, the digital PIV recording is divided in small areas called “interrogation windows”. The local 2C-displacement vector of the particle images between the two illuminations is determined for each interrogation window by means of a spatially statistical cross-correlation function, defined in Box 1. Given the time interval between the two laser pulses and the image magnification obtained from camera calibration, the projection of the local flow velocity vector onto the plane of the light sheet, attributed to the center of the interrogation window, can then be deduced. Neighboring interrogation windows can be partially overlapping in order to reduce the spacing between two vectors in the resulting vector grid. Typically, a 50% overlap is used, which doubles the number of vectors in each direction and thus quadruples the total number of vectors.

Figure 1 - Typical PIV setup

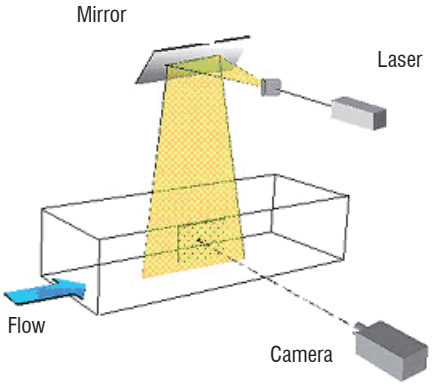

In standard PIV, though several types of laser sources are suitable, the most commonly used is the pulsed Neodyme-YAG (Nd:YAG) laser, doubled in frequency (532 nm). Pulse duration is typically 5-10 ns, and repetition rate is on the order of 10 Hz. Laser energy can reach 400 mJ/pulse. PIV systems are made of two independent laser cavities, but the laser beams should be superimposed in the near- and far-fields so that the two laser sheets illuminate the exact same area.
In most cameras, digital image recording is done via a CCD (Charge-Coupled Device) sensor which converts photons to an electric charge based on the photoelectric effect. The CCD sensor consists of many individual sensors that are arranged in a rectangular array. Each pixel has a size on the order of 10x10 μm. Their repetition rate in PIV double frame mode is on the order of 10 Hz.

Box 1 - Cross-correlation of a pair of two singly exposed recordings

Let $\boldsymbol{X}_i$ be the position vector and $\boldsymbol{x}_i$ the image position vector of particle i in the first exposure, respectively, related by $\boldsymbol{X}_i = \boldsymbol{x}_i / M$, where M is the magnification factor.

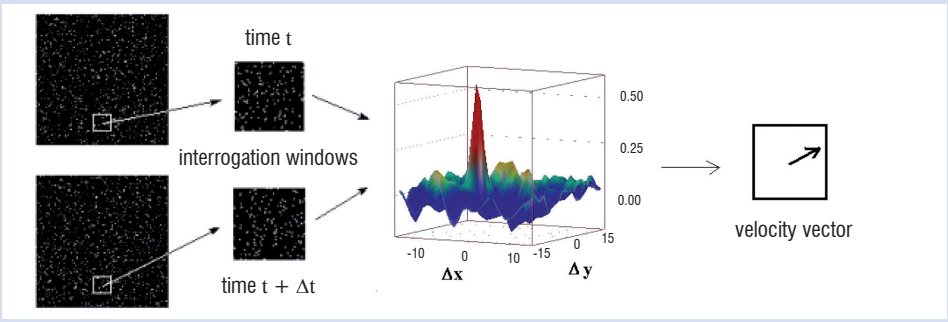

The image intensity field of the first exposure may be expressed by:

$$I(\boldsymbol{x}) = \sum_{i=1}^{N} V_0(\boldsymbol{X}_i)\,\tau(\boldsymbol{x} - \boldsymbol{x}_i)$$

where $V_0(\boldsymbol{X}_i)$ is the transfer function giving the light energy of the image of an individual particle i inside the interrogation volume and its conversion into an electronic signal, and $\tau(\boldsymbol{x})$ is the point spread function of the imaging lens, which is commonly considered to be Gaussian in both directions of the plane.
Assuming that between the two exposures all particles inside the interrogation window have moved with a same displacement vector $\boldsymbol{\Delta X}$, the image intensity field of the second exposure may be expressed by:

$$I'(\boldsymbol{x}) = \sum_{j=1}^{N} V_0'(\boldsymbol{X}_j + \boldsymbol{\Delta X})\,\tau(\boldsymbol{x} - \boldsymbol{x}_j - \boldsymbol{\delta x})$$

where $\boldsymbol{\delta x}$ is the particle image displacement, which can reasonably be approximated by $\boldsymbol{\Delta X} \cong \boldsymbol{\delta x}/M$
The cross-correlation of the two interrogation windows is defined as:
$R(\boldsymbol{s}) = \langle I(\boldsymbol{x})\, I(\boldsymbol{x}+\boldsymbol{s}) \rangle$, where $\boldsymbol{s}$ is the separation vector in the correlation plane, and $\langle\ \rangle$ is the spatial averaging operator over the interrogation window.
R can be decomposed into three parts:

$$R(\boldsymbol{s}) = R_C(\boldsymbol{s}) + R_F(\boldsymbol{s}) + R_D(\boldsymbol{s})$$

where R_C is the correlation of the mean image intensities, and R_F is the fluctuating noise component, both resulting from the $i \neq j$ terms. The displacement-correlation peak R_D represents the component of the cross-correlation function that corresponds to the correlation of images of particles from the first exposure with images of identical particles present in the second exposure ($i = j$ terms). This peak reaches a maximum for $\boldsymbol{s} = \boldsymbol{\delta x}$. Therefore, the determination of the location of this maximum yields $\boldsymbol{\delta x}$, thus $\boldsymbol{\Delta X}$. This location is commonly obtained through systematic exploration in the interrogation window by using Fast-Fourier Transform algorithms for computing cross-correlation. In the general case when all particles inside the interrogation window do not have uniform velocities (turbulence, velocity gradients), the location of the maximum yields the most probable displacement within the interrogation window. The value of $\boldsymbol{s}$ is determined with sub-pixel accuracy from correlation data interpolation, obtained through a fit of these data to some modeling function (e.g. Gaussian profile).

Although PIV relies on a simple principle, care should be taken in its practical implementation in order to obtain a reliable measurement and reduce uncertainties (see Box 2). The major asset of the PIV technique is its capacity to deliver a quantitative and instantaneous measurement of the velocity not only at one point, like Laser Doppler Velocimetry, but over a whole plane simultaneously: both visualization and quantification of the 2D flow structure become available. This, together with advances in electronic imaging and computing tools, explains its success over the past two decades.

Computation of the cross-correlation function

The computation of the cross-correlation function forms the heart of most commercially available data processing software and is commonly based on Fast-Fourier Transform (FFT) algorithms. Nowadays, most of them are iterative and based on an initial evaluation of velocity vectors using large interrogation windows, associated with a high SNR due to the large amount of particles taken into account in the statistics, but with poor spatial resolution. These velocity vectors and their gradients can then be used in the next step to adequately shift and deform the interrogation windows in each of the two exposures in order to reduce in-plane loss of correlated particle images. The interrogation window size is also progressively reduced to reach a final size of 32x32 or 16x16 pixels in practice, depending upon the density of particle images. Processing algorithms have been constantly developing with additional features aimed at enhancing signal-to-noise ratio (SNR) and removing spurious vectors. Recent efforts have mainly focused on improving spatial resolution by using adaptive interrogation windows parameters (size, shape, orientation). In particular, Theunissen et al. [13] reported, for cases when the interest lies in the mean flow field, an original scheme based upon statistical adaptivity, i.e. taking into account ensemble statistics over an entire image set.
Pre-processing is usually applied to raw images prior to cross-correlation computation in order to enhance contrast, reduce background noise (e.g. generated by particles deposits on windows), or homogenize particle intensities in order to avoid the bias of the cross-correlation function towards large particles. Following vector computation, post-processing operations are used to remove spurious vectors. This paper cannot cover all of the available declinations of PIV processing algorithms, so for specific detailed information the reader is invited to consult the references recommended in the introduction.

Principles of stereoscopic PIV (3C-PIV)

Adding a second camera to the setup, and arranging both cameras with different viewing axes, provides access to the otherwise unknown third component of the velocity vector, perpendicular to the laser light sheet and usually referred to as the out-of-plane component. This technique, known as stereoscopic PIV, can also reduce measurement uncertainty for the two in-plane components compared to a 2-C PIV setup, by accounting for the perspective projection caused by the displacement of the particles within the laser sheet thickness. Because what is measured when using only one camera is the projection of the local flow velocity vector onto one plane in the light sheet, the deduced displacement vector of the particle images results from two contributions: the in-plane displacement to be measured, but also the projection onto the plane of the out-of-plane component of velocity. In other words, the displacement of a particle animated with a purely out-of-plane velocity would be erroneously interpreted as a non-zero in-plane displacement. Note that this error is unrecoverable, although potentially significant in a highly three-dimensional flow.
By using two cameras with different viewing angles, projections of the velocity vector are obtained in two planes and in-plane can be differentiated from out-of-plane displacements. Whenever space and optical access constraints allow, the usual practice is to install the cameras so that the opening angle between them approaches 90°, as in this configuration the measurement uncertainty for the out-of-plane component is minimum and similar to the uncertainty for in-plane components. In order to obtain a satisfying image quality toward the edges of the field-of-view, the lens principal axis should be aligned with the principal viewing direction when the viewing direction is different than 90°. To make sure that the complete image is in focus, the plane of the CCD sensor should be tilted according to the Scheimpflug criterion, in which the image plane, lens plane and object plane intersect in a common line. In practice, this is performed by mounting the camera on a so-called Scheimpflug adaptor, which allows it to rotate with respect to the lens.
This optical arrangement has the side-effect of introducing a strong perspective distortion, which means that the magnification factor is no longer constant across the field-of-view. Therefore, the full spatial calibration matrix has to be determined for each camera. Quality of calibration is a key prerequisite for measurement reliability in stereoscopic PIV. The usual calibration procedure consists in taking several images of a flat calibration grid, placed first in the light sheet plane, then in a few other parallel planes. Based upon these images, a fit mapping function is computed for each camera and is used to dewarp raw particles images, i.e. to perform a back-projection in order to convert image coordinates into true “world” coordinates. Recent work performed at Onera has contributed to significant improvements

Box 2 - Measurement uncertainties in PIV

A reliable quantification of uncertainties is of prime importance for utilizing and interpreting experimental data, for PIV as much as for other metrological means. Even though numerous significant papers have already been published on this topic (e.g. see [10-11]), most of them focus on one particular cause of uncertainty, such as the presence of velocity gradients inside interrogation windows. Such studies are essential for selecting the best operating parameters to be implemented. However, the values they provide are not alone sufficient for a global estimation of an error bar for each computed velocity vector. In particular, many experimental studies indicate a displacement uncertainty of 0.05-0.1 pixel; however, this uncertainty refers only to the determination of the position of the correlation peak through sub-pixel interpolation of the correlation data [12]. As part of its quality management system processes, in 2007 Onera initiated an ambitious work program for a global and systematic assessment of measurement uncertainties in PIV. This work is still in progress, but preliminary results have already provided orders of magnitude for the relative significance of sources of uncertainty in the case of 2C-PIV: roughly 90% of the total uncertainty comes from the determination of the displacement in pixels from raw images; roughly 10% is due to camera calibration; compared to these causes, the uncertainty on the time interval between the two laser pulses is negligible.

in this field, leading to a new, more accurate and easier-to-use calibration procedure (Box 3). Finally, the calibration data obtained from the calibration grid can be further improved to account for the slight residual misalignment of the calibration plate with respect to the light sheet. The principle of this method, often referred to in the literature as "self-calibration", is to detect and correct small discrepancies between de-warped images recorded by the two cameras at the same time, which should contain identical information. Its implementation is based upon the computation of the cross-correlation function inside interrogation windows between these images (similarly to a standard PIV computation, see § "Computation of the cross-correlation function"), which results in disparity vectors being brought iteratively to a near-zero value.
Once calibration parameters have been determined for both cameras, two corresponding two-component vector fields can be computed from the de-warped images. The three velocity components can be deduced from these vector fields by solving a system of linear equations. The velocity vectors and their gradients can be utilized within an iterative scheme, in order to adequately shift and deform the interrogation windows in the next step.

Applications of PIV at Onera

Considering the large variety of experimental studies in its laboratories in which knowledge of the velocity field is of prime interest, the PIV technique has found at Onera a natural environment where it has been thoroughly implemented. Several research groups are equipped with PIV systems, in which data acquisition and processing software is either commercial or home-developed. The fields of application cover fundamental or applied aerodynamics and energetics for non-reacting or reacting flows. In this section, the advantages of the PIV technique are illustrated through different studies performed in Onera laboratories for non-reacting or reacting flows, and various issues raised by the nature of fluid, flow dynamics, spatial and temporal resolutions, as well as data utilization, are examined.

Multiple-camera PIV in aerial wakes of flying aircraft models

In the last decade, a lot of research on the wake vortex characterization and their alleviation has been carried out jointly by Onera and DLR [15, 16]. Vortex sheets shed off the wings of large aircraft, roll up, and organize into a multiple-vortex system in the aircraft's wake. Such large-scale coherent vortical structures usually are considerably stable and energetic. If an aircraft passes through this phenomenon during its takeoff or landing, it can dangerously affect its flight. As a consequence, regulatory separation distances have been imposed between the aircrafts. This safety regulation limits the airport's capacities. Therefore, the alleviation of wake vortices remains an important issue in commercial aviation.
The experimental campaign presented here was carried out in close cooperation with DLR. In the framework of the AWIATOR program, the main objectives of these tests were, on the one hand, to characterize the alleviation of wakes generated by different aircraft models and for various high lift configurations, and, on the other, to demonstrate the benefits of wing devices and span loading. This experimental campaign was carried out in the Onera B20 Free Flight Laboratory, shown in Figure 2. Compared to wind tunnels, in this facility the evolution of wakes can be studied from the near-field to far-field (from 0 to 100 wingspans). In this laboratory, non-motor-

Box 3 - Polynomial calibration versus pinhole calibration

The PIV community often uses polynomial calibration while the Computer Vision (CV) community only uses pinhole calibration (see Box 5 in [30]). Polynomial calibration can be implemented easily and usually gives a calibration error slightly lower than the pinhole method. However, it does not model the real world. During a 3-C PIV test, it was found that a significant error can be introduced by polynomial calibration [14]. This was demonstrated by comparing two overlapping PIV velocity fields, for which on the overlapped area the results were identical with pinhole calibration but different with polynomial calibration.
The reason is that the image velocities (see figure below) are equivalent to the spatial derivatives of the calibrations. The two following matrixes provide the 3-C velocity components from the two 2-C image velocity components. It can be seen that the differences are around 3% on the W component, the last line.

$$\begin{pmatrix} u \\ v \\ w \end{pmatrix}_{poly.} = \begin{bmatrix} 0.0726 & 0.0000 & 0.0743 & 0.0001 \\ -0.0006 & -0.0525 & 0.0008 & -0.0523 \\ -0.0718 & -0.0001 & 0.0714 & 0.0002 \end{bmatrix} \begin{pmatrix} u_1 \\ v_1 \\ u_2 \\ v_2 \end{pmatrix} \qquad \begin{pmatrix} u \\ v \\ w \end{pmatrix}_{pinhole} = \begin{bmatrix} 0.0736 & 0.0000 & 0.0734 & 0.0001 \\ 0.0000 & -0.0525 & 0.0001 & -0.0523 \\ -0.0742 & 0.0001 & 0.0739 & 0.0001 \end{bmatrix} \begin{pmatrix} u_1 \\ v_1 \\ u_2 \\ v_2 \end{pmatrix}$$

This surprising result can be explained: polynomial calibration uses too many parameters, which gives an improved calibration fit but creates unrealistic effects, enhanced by the derivative nature of the previous matrixes.
The pinhole model is then highly recommended and has just been extended at Onera in order to take into account thick window effect and even medium changes (air/glass/water) along the viewing direction. Combining it with the CV calibration method (see Box 5 in [30]), which does not require translation of the calibration body at known z-locations (Soloff's method), makes the pinhole model more reliable and easier to use than polynomial calibration.

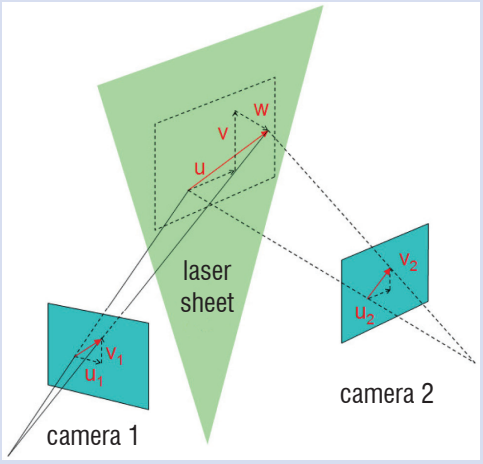

Projected velocities on the two cameras images

ized free flying scaled models are propelled by means of a pneumatic catapult via a trolley. Once launched, the model flies freely, i.e. without any wall or mounting interference, in a 90 m long, 20 m wide and 20 m high observation area. At the end of its free flight, it lands in a recovering system. An example of an aircraft model is shown in Figure 2 (wingspan b ≈ 2.1 m and weight M ≈ 23 kg).
In order to investigate a very large field of observation (≈ 1.7 m²) without loss of spatial resolution, 12 high-resolution PIV cameras were used for recording images (see Figure 2). This solution meant that the small eddies in the near field could be measured accurately as well as the coherent vortical structures in the far field. The arrangement of the cameras was chosen to provide a fine resolution in the center region of the wake and a coarser one in the outer regions. During flight, the wake of aircraft model has a descending movement. In order to follow this displacement, both light sheet optics and cameras were mounted on a traversable gantry so as to be translated simultaneously. The flow tracers were DEHS (synthetic oil) particles. The mean size of these droplets was around 1 micrometer. The flow was only seeded 15 minutes before each run of the model. The illumination of the particles in a very large field required a particularly high energy density in the light sheets. Therefore, two frequency-doubled, double-cavity high-energy (300 mJ/pulse) Nd:YAG lasers were used, instead of only one, in order to double the energy in each light sheet formed at the two exposures. Under these conditions, the energy was 600 mJ in each of the two light sheets. As the cameras are limited in repetition rate, PIV images were recorded at 3 Hz, which was the largest value compatible with the capabilities of all components of the PIV recording setup. During one launch, each camera recorded around 40 PIV pairs of images.
Figure 2 shows two examples of velocity fields. In the left one, obtained in the near-wake field, the two main vortices generated by the wing tip and the tail are clearly visible. However, a single coherent vortical structure is detected in the second velocity field, measured in the mid-wake field. Each velocity map includes around 60,000 instantaneous velocity vectors. Three axial vorticity fields are presented in Figure 2. The left one, obtained in the near-wake field of the model (X/b<2), reveals the formation of the different vortices mainly generated by the Horizontal Tail Plane (HTP), flaps (Inner/Board Co-rotating Vortex) and wing tips. After a few wingspans (extended near-wake field), the roll-up and merging of dominant vortices occurs, gradually leading to one main vortex. In the mid-wake field of the model (10 < X/b < 100), the axial vorticity map (on the right in Figure 2) shows the lingering resulting vortex which drifts downwards in the atmosphere. The full post-processing of the whole data sets was used not only to determine the trajectory, size and intensity of individual vortices detected (see figure 2, [17, 18]), to follow in detail the wake alleviation in all model configurations investigated, but also to evaluate quantitatively the efficiency of different wing devices tested.
During another campaign in the B20 Free-Flight Laboratory, PIV and LIDAR measurements were performed simultaneously. Comparisons between these two optical measurement techniques are presented in references [18] and [31].

Mean and turbulence measurements of wake vortices

In the wake vortices generation process, the initial roll-up vortex is due to the variation of the circulation distribution along the wingspan. Many experimental studies have been carried out on wake vortices, most of them in the near wake [19]. Jacquin and al. [20] investigated the extended near wake of a small scale A300 up to 9 wingspans downstream by the means of LDV and hotwire probe. The aim of the experimental study presented here was to characterize the vortex roll-up behind a generic wing equipped with an inboard flap deflected at different angles. A half-wing model of 75 mm chord, 150 mm half-span (aspect ratio equal to 4), rounded wingtip and NACA0012 wing section was tested in the Onera/Thales hydrodynamic tunnel (upstream velocity: 4 m.s^{-1}; Reynolds number based on chord: around 3 10^5) shown in Figure 3. The flap was 80% of the half-span large and 30% of the chord long. The flap angle could be set to 0° (clean case), 4°, 6° or 8°. The double-cavity pulsed laser, cameras and sheet optics of a stereoscopic PIV system were mounted on a traversable gantry in order to investigate several cross plane configurations, up to almost 9 wingspans downstream. The cameras were installed on both sides of the test section under a symmetrical configuration. The water flow was seeded with silver-coated hollow glass spheres (mean diameter: 10 microns). In this experiment, the presence of internal water prisms induced distortion effects on the recorded images. To correct these, an original and efficient solution was adopted: external water prisms were installed close to the windows.
For all angles of incidence investigated, the mean fields of the three velocity components, of the axial vorticity, and the six Reynolds stresses were successfully measured, as shown by the color maps represented in Figure 3. However, turbulence measurements carried out in a wind or a water tunnel are altered by a phenomenon called vortex wandering, which is a slow side-to-side movement of a vortex, probably due to a receptivity of the background turbulence of the facility. Devenport and al. [21] proposed a method to remove the wandering effects from hot wire measurements, in particular on the turbulence by high-pass filtering. PIV, which supplies instantaneous velocity fields, was used to develop an original and more objective procedure [22]. The vortex location was first detected in each instantaneous field based upon the so-called λ_2 criterion computed from the gradient tensor [23]. Assuming that the vortex has a solid motion, the average and standard deviation fields were then calculated after translating the instantaneous fields so that each instantaneous vortex center is at the same location. Taking vortex wandering into account leads to a dramatic correction of the turbulence levels in the vortex center, as shown by the plots of Root Mean Square (RMS) values in Figure 3, and explains why important peaks of turbulence are usually reported in the literature. This experiment demonstrated the great potential of the PIV technique for the qualification of wake vortices in the presence of the wandering phenomenon. Indeed, this optical diagnostic technique is the only one which is able to provide instantaneous velocity fields, required to correct this random effect encountered in aerodynamic or hydrodynamic facilities.

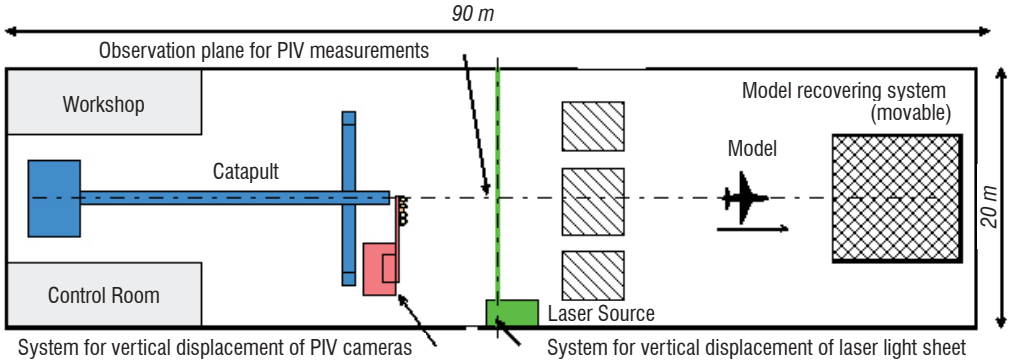

Schematic View of Onera B20 Free-Flight Facility and PIV setup

Large Transport Aircraft (LTA) Model

12 PIV cameras mounted on rails

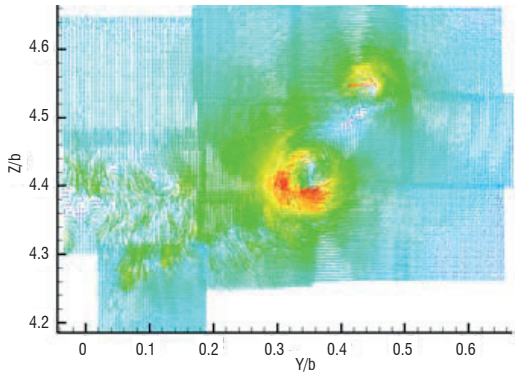

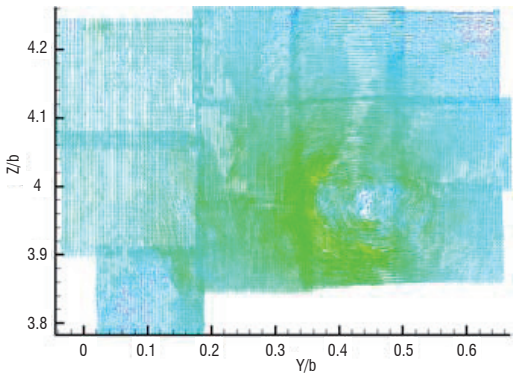

Velocity fields measured at longitudinal locations X/b= 1.3 and 30.4 - X: longitudinal distance downstream of the aircraft model, b: wingspan.

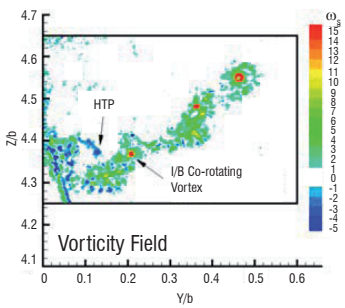

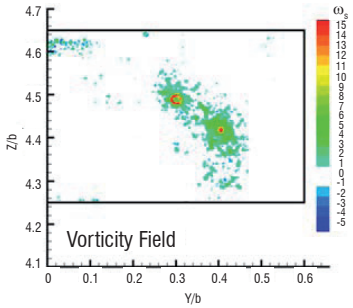

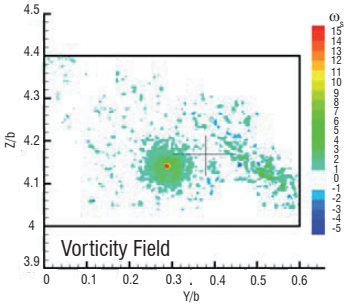

Axial vorticity fields at longitudinal locations X/b=1.3, 4.5 and 14.2 [18]

Figure 2 - Multiple-camera PIV in aerial wake of flying aircraft model

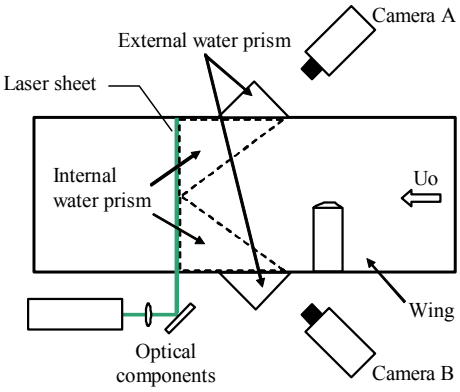

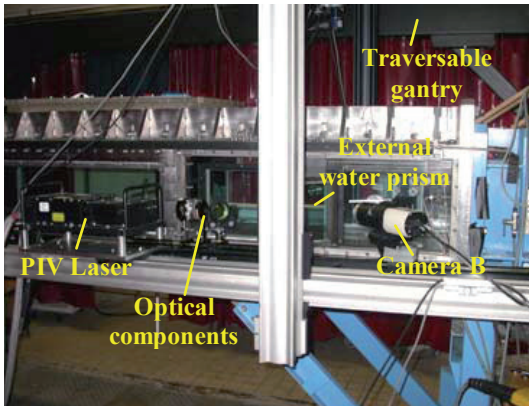

Implementation of the stereoscopic PIV technique in Onera hydrodynamic tunnel (top view and right side view)

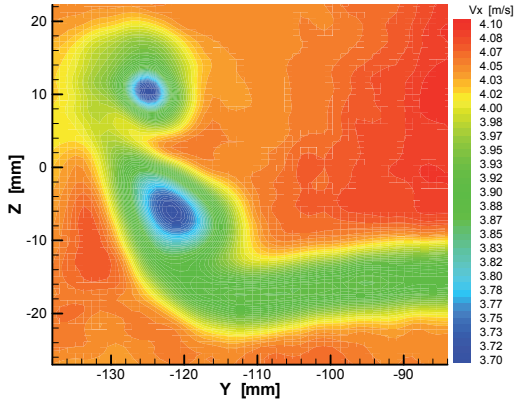

Axial velocity at X = 1.3b

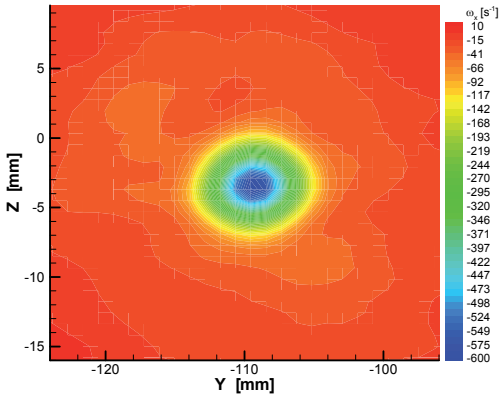

Axial vorticity at X = 3b

Mean fields in two cross planes. Angle of attack: 1.25°. Flap angle: 4°. X: distance downstream of the trailing edge; b: wingspan

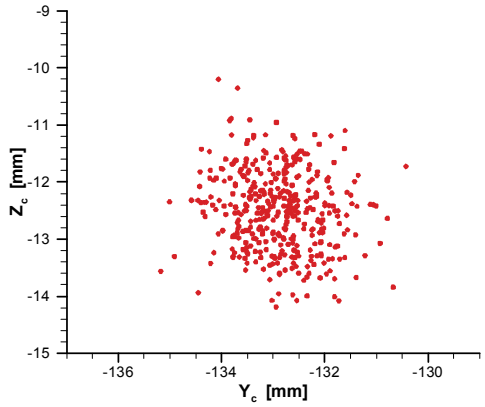

Instantaneous positions of the vortex center (400 samples)

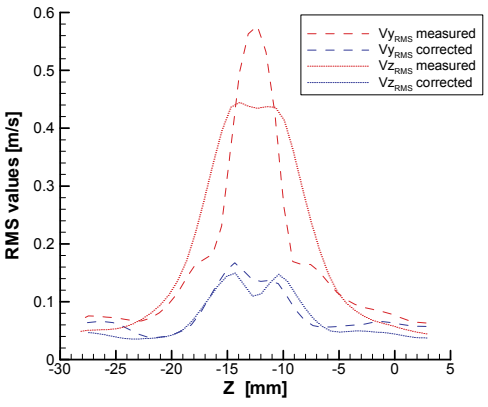

Effect of wandering correction on the transverse RMS values

Example of vortex wandering and effects of the correction. Angle of attack: 5°. Flap angle: 0°

Figure 3 - Mean and turbulence measurements of wake vortices

Thermo-acoustic flame instabilities in high turbulence flow

The purpose of this study [24] was to investigate low-frequency combustion instabilities in a model lean-premixed stepped combustor. Lean-premixed combustion has become one of the most promising means of meeting stringent environmental requirements for the reduction of NOx emissions produced by gas turbine engines. However, operating under lean premixed conditions often leads to the occurrence of undesirable combustion-driven pressure oscillations and intense heat release fluctuations that can severely damage the combustor or turbine hardware. The specific feature of this study, compared to most of research works published in the literature, was that it used high turbulence flow conditions representative of industrial combustors. Figure 4 shows a photograph of the methane/air flame anchored at the step in the combustion chamber, illuminated by one of the two superimposed vertical laser sheets used for PIV in the axial plane. Micronic solid magnesium oxide (MgO) seeding particles were used as flow tracers due to their capacity of withstanding the high-temperature reacting environment. For an unstable flame, the power spectrum of the unsteady pressure signals showed a dominant 154 dB peak at 66 Hz, corresponding to the ¼-longitudinal acoustic wave of the inlet duct. This raised the following question: how can a cyclic phenomenon at 66 Hz be studied using a standard PIV system with a repetition rate of less than 10 Hz? The usual answer is to phase-lock the PIV data acquisition with the signal from a high-frequency sensor, e.g. in our experiment the unsteady pressure trace. By using adequate time delays to trigger the PIV data acquisition with respect to the time reference from the pressure trace, the full cycle can be resolved. This procedure can be repeated at the PIV system repetition rate in order to perform a statistical analysis of all measured instantaneous vector fields. Though this method is frequently used, it requires the investigated cycle to be perfectly constant in frequency and amplitude, since lasers require a constant frequency trigger. This was not the case in our experiment, in which the pressure signals were highly modulated in frequency (in the range 55-80 Hz) and amplitude. Therefore, an alternative solution was adopted, which consisted in synchronizing the PIV acquisition with that of a digital high-speed (4,000 Hz) camera recording the chemiluminescence signal of the OH* radical, used as a natural tracer of the flame front. This method allowed to identify the instant, pressure, and flame location in the cycle to which each measured velocity field corresponded. An example of an instantaneous PIV velocity field synchronized with high-speed images, taken as the flame propagated downstream toward the step before re-attachment, is provided in Figure 4. This result showed that this motion was associated with the formation of a strong vortex behind the step and an induced acceleration near the step edge. The PIV technique was also particularly well-suited to this study due to its large dynamic range, which meant that it could measure the highly fluctuating levels of velocity (from 0 to 200 m/s) revealed during the experiments.

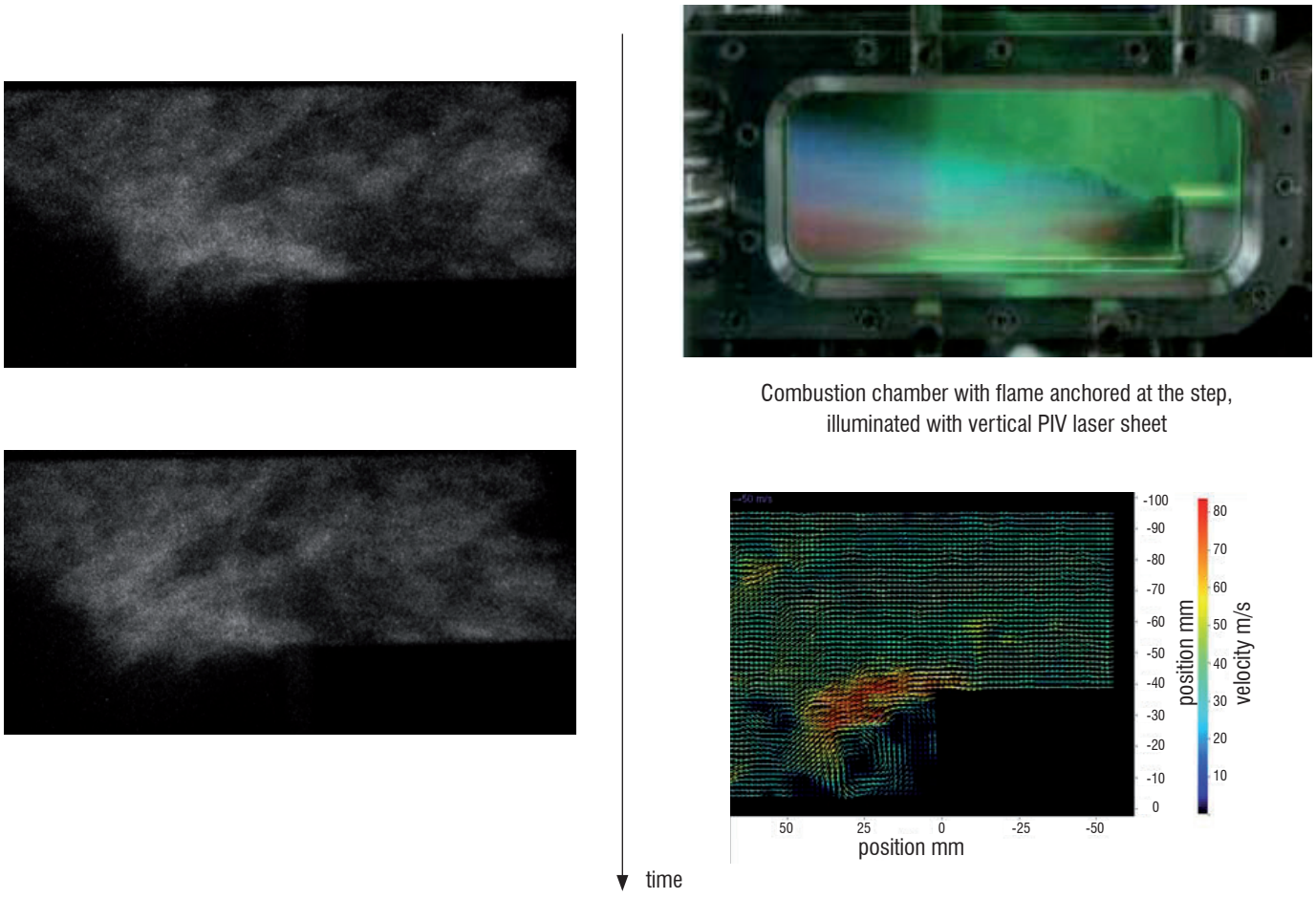

Combustion chamber with flame anchored at the step, illuminated with vertical PIV laser sheet

Instantaneous PIV velocity field synchronized with high-speed OH* chemiluminescence images at 4,000 Hz.

Figure 4 - Thermo-acoustic flame instabilities in high turbulence flow

Recent advances in PIV

Time-Resolved PIV

The technological limits of PIV have been pushed further into the distance by the still ongoing progress in laser technologies and electronic imaging systems. In particular, the new high repetition rate lasers and cameras available today have led to the development of time-resolved PIV (often referred to as TR-PIV in the literature). Some high-speed cameras available today, based on CMOS (Complementary Metal Oxide Semiconductors) sensors, can reach a repetition rate of more than 80 kHz (with a resolution reduced to 256x256 pixels), i.e. a PIV repetition rate of more than 40 kHz (2 images per PIV acquisition). The major drawback of these cameras with respect to standard PIV CCD cameras is a larger pixel size, slightly less than 20x20 μm, but this difference has been significantly decreased in recent camera models. TR-PIV systems are currently limited by laser energy: a few mJ/pulse at 10 kHz for a high-speed Nd:YLF laser, versus up to 400 mJ/pulse at tens of Hz for a Nd:YAG laser used in standard PIV (see Figure 1). In addition, high-speed laser pulse widths increase with repetition rate and range between 100 and 300 ns: this is much higher than the 5-10 ns pulse width of a Nd:YAG laser, and can be a severe limitation when investigating high-speed flows. Despite these drawbacks, the recent success of TR-PIV systems can be explained by the jump in time resolution from the Hertz to the kilohertz range that they provide. One particular PIV hardware system can also be used in a broad frequency range, typically from 1 to 10 kHz: as the product of repetition rate and energy per pulse stays roughly constant over the operating range, this offers some flexibility for finding the best compromise between energy and repetition rate based upon the experimental constraints. Technological progress is so fast that, according to some researchers [25], TR-PIV could replace standard PIV in a few years.Time-resolved PIV has opened the way to quantitative measurement of velocity fields for unsteady flows or transient phenomena, which is a requirement for validating computation codes [32,33]. Until now, the highest operating (i.e. with sufficient energy per pulse) repetition rates of high-speed lasers have been limited to 20 kHz, which is borderline for resolving the smallest time scales of turbulence in many practical flows: Laser Doppler Velocimetry (up to several tens of kHz repetition rate) is still the most suitable optical diagnostic technique for accessing such information. However, this could change in the very near future, as highest available repetition rates have kept increasing very fast recently.

Tomographic PIV

A natural development of the PIV technique has been its extension to the third dimension in space, i.e. from a 2D planar to a 3D volumetric technique. Several different 3D techniques now exist: holographic PIV, scanning PIV, dual plane PIV, 3D PTV (Particle Tracking Velocimetry), defocusing PIV and, more recently, tomographic PIV [26, 27]. This latter technique is a very powerful one, compared to the others, that offers the simultaneous advantages of being fully volumetric, truly instantaneous and based on fully digital data recording and analysis. It is based on an extension of the stereoscopic PIV concept by using the principle of tomographic volume reconstruction. The 3D light intensity field of the illuminated particles is reconstructed for each voxel (the 3D equivalent to a pixel) from the images of typically four cameras viewing from different angles, by using a tomographic reconstruction algorithm. The entire volume is kept in focus by using a relatively small lens aperture (typically f-numbers > 8) and applying the Scheimpflug condition (see § "Principles of stereoscopic PIV"). The particle displacement (hence velocity vector) within an interrogation volume is then obtained by the 3D cross-correlation of the reconstructed particle distributions at the two exposures. Combining TR-PIV hardware under a tomographic PIV arrangement leads to time-resolved tomographic PIV, which is used to obtain what ultimately most fluid mechanics researchers look for: a full sequence showing the time-resolved evolution of the three-component velocity vectors inside a volume. Reference [28] is a particularly good illustration of this technique's potential. It enabled the researchers to carry out for the first time a topological investigation of the flow structures in a turbulent boundary layer, within a temporally and spatially highly resolved Lagrangian and Eulerian frame.

The MEMFIS research project at Onera

The importance of the PIV technique in many research labs and the current development of more advanced techniques, presented previously, can generate extremely large amounts of data, which raises the question of using the adequate numerical data processing. Compared to progress recently made in the experimental setting and acquisition devices, data processing in most commercial PIV systems still relies on window correlation techniques dating back from the 80's, and seems rather cautious about recent developments in motion estimation techniques originating from the Computer Vision community. The MEMFIS project (which stands for "Methods for Movements and deFormations Estimations by Imaging and Stereoscopy"), initiated in 2007 by the Modeling and Information Processing Department at Onera, aims to spread these developments to Onera's physicists both in the Fluid Mechanics and Energetic branch and in the Materials and Structures branch. MEMFIS promotes federative research in three main directions:

Algorithm

Study of fast and parallel techniques for flow field computation (multigrid, domain decomposition, etc.), to pave the way for massive dataset processing in TR-PIV and 3D tomographic PIV. Reference [34] presents recent work conducted at Onera on this subject.

Variational approaches for flow field estimation

Although many iterative refinements and post-processing are included in modern software to extend their use, window correlation methods are fundamentally based on the prior assumption that the flow field investigated is locally uniform. Such an assumption is necessary for increasing the signal-to-noise ratio, at the cost of a bias in the deduced velocity, which is a form of spatial regularization of the flow field estimation. Recently, new regularization principles based on variational approaches have been proposed, some of them dedicated to fluid dynamics [29]. These techniques, which are studied in the MEMFIS project, can be considered as an attempt to bridge the gap between experimental data processing and numerical simulation.

Post-processing and PIV data interpretation

Up to now, PIV data have been mostly used in terms of temporal statistics (average and fluctuations). Post-processing algorithms to

be developed in the frame of the MEMFIS research project open the way to an interpretation in terms of instantaneous flow structures, hence a more adequate comparison with newly developed LES-based (Large Eddy Simulation) computation codes [32].
Regarding the latter subject, a topic of interest to many applications is the detection of vortices in the flow field. Previouly (see § "Mean and turbulence measurements of wake vortices") was illustrated how a detection scheme can take the effects of wandering on turbulence measurements into account and correct them. Applied to time-resolved PIV data, algorithms dedicated to vortices detection should also allow the temporal tracking of these vortices.Therefore, the MEMFIS research project constitutes an excellent interface between the advances in PIV supported by new technologies on one side, and those in numerical simulations on the other side.

Conclusion

The very high potential of the PIV technique has been illustrated through some experimental studies performed at Onera. The examples presented show that this technique can provide detailed, qualitative and quantitative information on flow structure and turbulence, whether in the wake behind a wing or inside a combustion chamber. Progress in laser technologies and electronic imaging systems has brought new innovative and powerful improvements to the technique. Time-resolved PIV allows flow unsteadiness investigation. Tomographic PIV extends digital PIV from the planar to the volumetric domain. Novel processing algorithms developed at Onera in the framework of the MEMFIS research project are possible answers to a more efficient data processing and a better use of the vector fields obtained ■

References

[1] L. DAVID and P. GICQUEL - *Evolutions de la technique PIV à travers quelques conférences internationales de 2000 à aujourd'hui*. Congrès Francophone de Techniques Laser, CFTL 2006, Toulouse, France, September 19-22, 2006.
[2] M. STANISLAS, J. WESTERWEEL, J. KOMPENHANS - *Particle Image Velocimetry : Recent Improvements*. Proceedings of the EUROPIV2 workshop held in Zaragoza, Spain, March 31, April 1, 2003.
[3] M. STANISLAS, K. OKAMOTO, C.J. KÄHLER - *Main Results of the First International PIV Challenge*. Measurement Science and Technology, Vol. 14, pp. R63-R89, 2003.
[4] M. STANISLAS, K. OKAMOTO, C.J. KÄHLER, J. WESTERWEEL - *Main Results of the Second International PIV Challenge*. Exp. Fluids, Vol. 39, pp. 170-191, 2005.
[5] M. STANISLAS, K. OKAMOTO, C.J. KÄHLER, J. WESTERWEEL, F. SCARANO - *Main results of the Third International PIV Challenge*. Exp. Fluids, Vol. 45, pp. 27-71, 2008.
[6] M. RAFFEL, C. WILLERT, J. KOMPENHANS - *Particle Image Velocimetry – A practical Guide*. Springer-Verlag Berlin Heidelberg, 1998.
[7] DLR PIV Course - *Application of Particle Image Velocimetry* – Theory and Practice. http://pivcourse.dlr.de/
[8] VKI Lecture series, http://www.vki.ac.be/
[9] Ecole d'Automne de Vélocimétrie et Granulométrie Laser en Mécanique des Fluides, http://www.afvl.ensma.fr/
[10] B. LECORDIER, M. TRINITÉ - *Accuracy Assessment of Image Interpolation Schemes for PIV from Real Images of Particle*. 13th Int. Symp. on Applications of Laser Techniques to Fluid Mechanics, Lisbon, Portugal, June 26-29, 2006.
[11] J. WESTERWEEL - *On Velocity Gradients in PIV Interrogation*. Exp. Fluids, Vol. 44, pp. 831-842, 2008.
[12] J. WESTERWEEL - *Theoretical Analysis of the Measurement Precision in Particle Image Velocimetry*. Exp. Fluids, Vol. 29, N°7, pp. S3-S12, 2000.
[13] R. THEUNISSEN, F. SCARANO, M.L. RIETHMULLER - *Statistical Adaptivity in PIV Interrogation for Mean Flow Estimation*. 14th Int. Symp. on Applications of Laser Techniques to Fluid Mechanics, Lisbon, Portugal, 07 -10 July 2008.
[14] Y. LE SANT, B. GARDARIN, B. LECLAIRE, P. GEFFROY, D. SOULEVANT - *Polynomial Calibration vs Pinhole Calibration*. 7th Int. Symp. on Particle Image Velocimetry, Roma, Italy, September 2007.
[15] E. COUSTOLS, L. JACQUIN, F. MOENS, P. MOLTON - *Status of Onera Research on Wake Vortex in the Framework of National Activities and European Collaboration*. European Congress on Computational Methods in Applied Sciences and Engineering, ECCOMAS 2004 Conference, Jyväskylä, Finland, 24-28 July. P. Neittaanmäki, T. Rossi, S. Korotov, E. Oñate, J. Périaux, and D. Knörzer (Eds.).
[16] E. COUSTOLS, L. JACQUIN, G. SCHRAUF, 2006 - *Status of Wake Vortex Alleviation in the Framework of European Collaboration: Validation Attempts Using Tests and CFD Results*. European Conference on Computational Fluid Dynamics, ECCOMAS CFD 2006, P. Wesseling, E. Oñate, J. Périaux (Eds).
[17] C.F.V. CARMER, R. KONRATH, A. SCHRÖDER, J.-C. MONNIER - *Identification of vortex pairs in aircraft wakes from sectional velocity data* - Exp. Fluids, Vol. 44, pp. 367-380, 2008.
[18] E. COUSTOLS, A. DOLFI-BOUTEYRE, A. GILLIOT - *Developments of PIV and Lidar Measurements for Wake Vortex Tracking at the Onera B20 free-Flight Facility*. Aerospace 08, Testing – Design – Manufacturing, European Ground Testing Instrumentation Symposium, Munich, Germany, April 15-16, 2008.
[19] J. S. CHOW, G. G. ZILLIAC, P. BRADSHAW - *Mean and Turbulence Measurements in the Near Field of a Wingtip Vortex*. AIAA Journal, Vol. 35, N°. 10, October 1997.
[20] L. JACQUIN, E. COUSTOLS, P. GEOFFROY, S. BRUNET, G. PAILHAS - *Experimental Study of the Vortex Wake Behind a A300 Airbus Model.* Technical report N° RT 14/2496 DAFE/Y, April 1998.
[21] W. J. DEVENPORT, M. C. RIFE, S. I. LIAPIS, G. S. FOLLIN - *The Structure and Development of a Wing-Tip Vortex*. J. Fluid Mech., Vol. 312, pp. 67-106, 1996.
[22] F.-X. VANDERNOOT, P. BARRICAU, H. BEZARD, H.-C. BOISSON - *Mean and Turbulence Measurements of Wake Vortices*. 14th Int. Symp. on Applications of Laser Techniques to Fluid Mechanics, Lisbon, Portugal, 07 -10 July 2008.
[23] J. JEONG, F. HUSSAIN - *On the Identification of a Vortex*. J. Fluid Mech. Vol. 285, pp. 69-94, 1995.
[24] V. SABEL'NIKOV, C. BROSSARD, M. ORAIN, F. GRISCH, M. BARAT, A. RISTORI, P. GICQUEL - *Thermo-Acoustic Instabilities in a Backward-Facing Step Stabilized Lean-Premixed Flame in High Turbulence Flow*. 14th Int. Symp. on Applications of Laser Techniques to Fluid Mechanics, Lisbon, Portugal, 07 -10 July 2008.
[25] R. HAIN, C. J. KÄHLER - *Advanced Evaluation of Time-Resolved PIV Image Sequences*. 6th Int. Symp. on Particle Image Velocimetry, Pasadena, California, USA, September 21-23, 2005.
[26] G.E. ELSINGA, F. SCARANO, B. WIENEKE, B.W. VAN OUDHEUSDEN - *Tomographic Particle Image Velocimetry*. 6th Int. Symp. on Particle Image Velocimetry, Pasadena, California, USA, September 21-23, 2005.
[27] F. SCARANO - *Tomographie en PIV: nouveaux développements et perspectives en vélocimétrie tridimensionnelle résolue dans le temps*. Congrès Francophone de Techniques Laser, CFTL 2006, Toulouse, France, September 19-22, 2006.
[28] A. SCHRÖDER, R. GEISLER, K. STAACK, B. WIENEKE, G.E. ELSINGA, F. SCARANO, A. HENNING - *Lagrangian and Eulerian Views into a Turbulent Boundary Layer Flow Using Time-Resolved Tomographic PIV.* 14th Int. Symp. on Applications of Laser Techniques to Fluid Mechanics, Lisbon, Portugal, 07 -10 July 2008.

[29] P. RUHNAU, C. SCHNÖRR - Optical Stokes Flow Estimation: an Imaging-Based Control Approach. Experiments in Fluids, Vol. 42, pp. 61-78, 2007.
[30] Y. LE SANT, B. AUPOIX, P. BARRICAU, M-C. MÉRIENNE, G. PAILHAS, P. REULET, Y. TOUVET - *Surface Mapping Methods. Aerospace Lab n°1*, December 2009.
[31] A. DOLFI-BOUTEYRE, B. AUGERE, M. VALLA, D. GOULAR, D. FLEURY, G. CANAT, C. PLANCHAT, T. GAUDO, C. BESSON, A. GILLIOT, J-P CARIOU, O PETILON, J. LAWSON-DAKU, S. BROUSMICHE, S LUGAN, L. BRICTEUX, B . MACQ - Aircraft Wake Vortex Study and Characterisation with 1.5 μM Fiber Doppler Lidar. Aerospace Lab N°1, December 2009.
[32] L. JACQUIN - *Scales in Turbulent Motions.* Aerospace Lab N°1, December 2009.
[33] F. DUPOIRIEUX - *Optical Diagnostics Used at Onera to Characterize Turbulent Reactive Flows and to Validate Aero- and Rocket Engine Combustor Modelling*. Aerospace Lab N°1, December 2009.
[34] G. LE BESNERAIS, F. CHAMPAGNAT, A. PLYER, R. FEZZANI, B. LECLAIRE, Y. LESANT - *Advanced Processing Methods for Image-Based Displacement Field Measurement.* Aerospace Lab N°1, December 2009.

Acronyms

CCD (Charge-Coupled Device)
CMOS (Complementary Metal Oxide Semiconductors)
CV (Computer Vision)
DEHS (Di-Ethyl-Hexyl-Sebacate)
DLR (Deustches zentrum fur Luft und Raumfahrt)
FFT (Fast-Fourier Transform)
HTP (Horizontal Tail Plane)
LDV (Laser Doppler Velocimetry)
LES (Large Eddy Simulation)
LIDAR (Light Detection And Ranging)
MEMFIS (Methods for Movements and deFormations Estimations by Imaging and Stereoscopy)
PIV (Particle Image Velocimetry)
2C-PIV (Two-Component PIV)
3C-PIV (Three Component PIV)
PTV (Particle Tracking Velocimetry)
RMS (Root Mean Square)
SNR (Signal-to-Noise Ratio)
TR-PIV (Time-Resolved PIV)

AUTHORS

Christophe Brossard received his Engineering Degree in Energetics from the "Institut National des Sciences appliquées" in Rouen, France, in 1991. He received his Doctoral Degree in Energetics from the University of Rouen in 1995. From 1996 to 2001, he worked at the Propulsion Engineering Research Center at Pennsylvania State University, USA. Since 2001, he has worked as a research scientist in the Fundamental and Applied Energetics Department at Onera, focusing on flow field characterization, in non-reacting or reacting environments, using optical diagnostic techniques (PIV, LDV, Phase Doppler). His current research addresses the investigation of swirl-stabilized flames using time-resolved PIV, and the post-processing of PIV vector fields for flow structures motion detection.

Jean-Claude Monnier received his doctoral degree in Mechanics from the University of Lille. Since 1990, he has been employed as a research scientist in the Applied Aerodynamics Department at Onera. He started with experimental work on problems of Fundamental Fluid Mechanics. For eighteen years, he has worked mainly on the development of Particle Image Velocimetry (PIV) and its use for aerodynamic applications and in large industrial scale wind tunnels. Since 1998, he has managed the PIV team of the Applied Aerodynamics Department.

Philippe Barricau graduated in solid state physics from the "Institut National des Sciences Appliquées". Since 1998, he has worked in the field of instrumentation applied to aerodynamics. He has developed the optical arrangement of a Doppler Global Velocimetry system. He has also implemented the PIV technique in various Onera facilities and used the oil film technique to measure skin friction in various flows. Since 2008, he has been working on the development of sparkjet actuators for flow control applications.

François-Xavier Vandernoot graduated as an engineer at Supaero (French Engineering School of Aeronautics and Space) in 2005. He developed a research activity on wake vortices within the aerodynamics laboratory. His student work was rewarded with the Ludwig Prandtl prize. After a Master of Research in Fluid Dynamics at the University of Toulouse, rewarded by the Onera prize for the best Master of Research project in 2005, and a training period, he continued to work at Onera for three years as part of a PhD on the experimental and numerical study of wake vortices. In 2009, he joined Airbus in the wake vortex team and now works on evaluating the criticality of wake vortex encounters.

Yves Le Sant Researcher at Onera since 1983. His first studies concerned wall interferences and the development of an adaptive test section. Then he was involved in applying and developing many measurements methods, such as heat flux assessment, temperature and pressure sensitive paints and model deformation. His current activities are in the field of image processing applications, such as in Particle Image Velocimetry.

Frédéric Champagnat graduated from the Ecole Nationale Supérieure de Techniques Avancées in 1989 and received a Ph.D. degree in physics from the Université de Paris-Sud, Orsay, France, in 1993. From 1994 to 1995, he held a Postdoctoral position with the Biomedical Engineering Institute, Ecole Polytechnique, Montreal, QC, Canada. Since 1998, he has been with the Onera, Chatillon, France. His main interests are in the field of spatio-temporal processing for space or aerial image sequences, in particular registration, motion estimation, super-resolution, and detection.

Guy Le Besnerais graduated from the Ecole Nationale Supérieure de Techniques Avancées in 1989 and received a Ph.D. degree in physics from the Université de Paris-Sud, Orsay, France, in 1993. He joined Onera in 1994, where he is now a senior scientist in the Modeling and Information Processing Department. His work concerns inversion problems in imagery and computer vision, with an emphasis on embedded perception for autonomous aerial robots.